ACS APPLIED MATERIALS & INTERFACES

Research Article

www.acsami.org

Spinel Manganese–Nickel–Cobalt Ternary Oxide Nanowire Array for High-Performance Electrochemical Capacitor Applications

Lu Li,[†] Yongqi Zhang,[‡] Fan Shi,[†] Yijun Zhang,[†] Jiaheng Zhang,[†] Changdong Gu,[†] Xiuli Wang,[†] and Jiangping Tu*[,†]

[†]State Key Laboratory of Silicon Materials, Key Laboratory of Advanced Materials and Applications for Batteries of Zhejiang Province, and Department of Materials Science and Engineering, Zhejiang University, Hangzhou 310027, China

[‡]Division of Physics and Applied Physics, School of Physical and Mathematical Sciences, Nanyang Technological University, Singapore 637371, Singapore

Supporting Information

ABSTRACT: Aligned spinel Mn–Ni–Co ternary oxide (MNCO) nanowires are synthesized by a facile hydrothermal method. As an electrode of supercapacitors, the MNCO nanowire array on nickel foam shows an outstanding specific capacitance of 638 F g^{-1} at 1 A g^{-1} and excellent cycling stability. This exceptional performance benefits from its nanowire architecture, which can provide large reaction surface area, fast ion and electron transfer, and good structural stability. Furthermore, an asymmetric supercapacitor (ASC) with high energy density is assembled successfully by employing the MNCO nanowire array as positive electrode and carbon black as negative electrode. The excellent electrochemical performances indicate the promising potential application of the ASC device in the energy storage field.

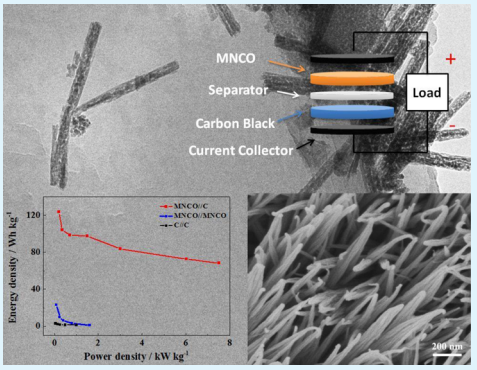

KEYWORDS: *ternary oxide, spinel structure, nanowires, hydrothermal method, electrochemical performance, asymmetric supercapacitor*

1. INTRODUCTION

Among various energy storage devices, electrochemical capacitors, also called supercapacitors, which is a new kind of energy storage device combining the features of conventional capacitors (high power density, long cycling life) and rechargeable batteries (high energy density), have been extensively studied.[1−14] Various applications in electric equipment and hybrid electric vehicles make electrochemical capacitors highly desirable. However, the energy density of existing supercapacitors is far from meeting the requirement. For practical applications, advanced supercapacitors must be developed with higher operating voltage and higher energy density without sacrificing power delivery and cycle life in the future.[15]

To improve the cell voltage and energy density of supercapacitors, considerable research efforts have been focusing on developing asymmetric supercapacitors (ASCs) comprising an electric double layer capacitor electrode (negative electrode) and a redox-active material electrode such as transition-metal oxides (positive electrode).[16−21] ASCs can make full use of the different potential windows of the two electrodes to increase the maximum operation voltage in the cell system, thus resulting in an enhanced specific capacitance and significantly improved energy density.[22] The negative electrodes are always carbon materials, while the positive electrodes widely employ metal oxides. Now the main focus of the ASC research is to develop advanced positive electrodes.

Nowadays, many nanostructured transition-metal oxides, such as Co_3O_4,[23−25] NiO,[26−29] MnO_2,[30−34] have been extensively investigated as pseudocapacitors and ASC electrodes. Among them, Co_3O_4 has attracted much attention for its high theory specific capacitance and high conductive property. However, its high cost and potential to contaminate the environment limit the applications of the Co_3O_4 electrode, so to partly replace the cobalt atoms with other elements while the nanostructure is maintained has been a feasible and promising strategy to address the issue. For instance, Zhang et al. synthesized mesoporous spinel $NiCo_2O_4$, which presented a high specific capacitance of 1619.1 F g^{-1} at a current density of 2.0 A g^{-1} and excellent cycling stability;[35] Gomez and Kalu fabricated a thin film binder-free $MnCo_2O_4$ electrode, and a specific capacitance around 832 F g^{-1} at a scan rate of 20 mV s^{-1} was obtained.[36] As far as we know, there are few reports about ternary composite oxide used in a supercapacitor electrode. As the atom radii of Mn, Ni, and Co are similar to each other, here, we introduce the elements Mn and Ni into Co_3O_4 to partly replace Co atoms, in order to obtain a Mn–Ni–Co ternary oxide (MNCO) without crystal structure change.

Received: July 25, 2014
Accepted: September 23, 2014
Published: September 23, 2014

Compared to Co_3O_4, the MNCO greatly reduces the cost and at the same time possesses better safety performance. Besides, it is expected to offer a synergistic effect on redox reactions, including contributions from cobalt, nickel, and manganese ions, compared to the corresponding single component oxides.

In this present work, the MNCO nanowire array directly grown on nickel foam is synthesized by a facile hydrothermal method, which yields the spinel structure reported for Co_3O_4. The MNCO electrode shows high specific capacitance and excellent cycling stability. At the same time, the ASC device is fabricated by using the MNCO nanowire array and carbon black as the positive and negative electrode, respectively, which also exhibits high energy and power density, as well as excellent electrochemical stability, indicating its promising application in energy storage.

2. EXPERIMENTAL SECTION

2.1. Preparation of Materials. All the reagents used in the experiment are of analytical grade and used as received without further purification. The cobalt nitrate, manganese nitrate, nickel nitrate, urea, and ammonium fluoride are obtained from Shanghai Chemical Reagent Co. All aqueous solutions were freshly prepared with high purity water (18 MΩ resistance).

MNCO nanowire array was synthesized by a facile hydrothermal method according to the following steps. The reaction solution was obtained by mixing 1 mmol of $Mn(NO_3)_2$, 1 mmol of $Ni(NO_3)_2$, 1 mmol of $Co(NO_3)_2$, 6 mmol of NH_4F, and 15 mmol of urea in 70 mL of distilled water under magnetic stirring for 30 min in air. Nickel foam substrates 3.5 × 5.0 cm^2 in size were pressed into thin plates under a pressure of 10 MPa and cleaned ultrasonically in ethanol for 20 min. The top sides of the substrates were uniformly coated with a polytetrafluoroethylene tape to prevent the contamination of the solution. Then the resulting solution was transferred into a 100 mL Teflon-lined stainless steel autoclave, and the nickel foam substrates were immersed into it. After 4 h at 120 °C, the autoclave was then naturally cooled down to room temperature. Subsequently, in order to remove the free debris and residual reactant, the hydroxide precursor film was washed with distilled water repeatedly. Finally, the precursor film was annealed at 350 °C in argon gas for 2 h to make a full transformation of precursor into the Mn−Ni−Co ternary oxide.

2.2. Characterization of Materials. The structure and morphology of the as-synthesized MNCO were characterized by X-ray diffraction (XRD, RIGAKU D/Max-2550 with Cu Kα radiation), scanning electron microscopy (Hitachi S-4800 equipped with GENENIS 4000 EDAX detector), and transmission electron microscopy (TEM, CM200, PHILIPS). The chemical composition of the product was examined by means of energy dispersive X-ray spectroscopy (EDX). The specific surface area was measured following the multipoint Brunauer−Emmett−Teller (BET) procedure from N_2 adsorption−desorption isotherms using an AUTOSORB-1-C gas sorption analyzer.

The electrochemical properties, as both supercapacitor electrode and asymmetric electrochemical capacitor, of the MNCO nanowire array grown on nickel foam were investigated. The mass of the active material loaded on the Ni foam substrate is 1.84 mg cm^{-2} and is obtained from the difference between the substrate mass measured before and after the hydrothermal-annealing procedure.

The electrochemical measurements of the MNCO nanowire array electrode were carried out in a three-electrode electrochemical cell containing 6 M KOH aqueous solution as the electrolyte with Pt foil and Ag/AgCl electrode as the counter and reference electrode, respectively. Cyclic voltammetry (CV) measurements were performed on a CHI660D electrochemical workstation (Chenhua, Shanghai, China) in the potential range of 0−0.5 V (vs Ag/AgCl) at scanning rates of 50, 20, 10, and 5 mV s^{-1}. The galvanostatic charge−discharge tests were conducted on a LAND battery program-control test system. The specific capacitance is calculated according to the following equation: $C = I\Delta t/M\Delta V$, where C (F g^{-1}) is the specific capacitance, I (mA) represents the discharge current, and M (mg), ΔV (V) and Δt (s) designate the mass of active material, potential drop during discharge, and total discharge time, respectively. The energy density (E) is calculated according to the equation $E = C\Delta V^2/2$, and the power density (P) is calculated according to the equation $P = E/\Delta T$.

The electrochemical measurements of the ASC device were carried out in a two-electrode electrochemical cell containing 6 M KOH aqueous solution as the electrolyte. The ASC was assembled using the MNCO as positive electrode, the carbon black electrode as negative electrode, and the cellulose acetate as separator. The scheme is shown in Figure S1 (see Supporting Information). Particularly, the negative electrode was prepared as follows: First, 90 wt % carbon black and 10 wt % polyvinylidene fluoride binder dispersed in 1-methylpyrrolidone solvent were mechanically mixed to produce a homogeneous paste. Then the mixture was coated onto the nickel foam substrate to form the electrode layer. Finally, the fabricated electrode was pressed and then dried at 60 °C for 12 h. The electrochemical performances of the ASC device were measured by the same procedure as mentioned above. All the electrochemical measurements were conducted at room temperature.

3. RESULTS AND DISCUSSION

3.1. Characterization. The structure of the precursor and the final product were characterized by XRD analysis. The XRD pattern of the precursor film is shown in Figure S2 (Supporting Information). Besides three strong peaks from the nickel foam substrate, all the reflection peaks of the precursor film can be indexed to cobalt hydroxide $Co(OH)_2$ (JCPDS 02-0925). After annealing treatment, the Mn−Ni−Co ternary oxide is formed by the substitution of Mn and Ni atoms for Co atoms in Co_3O_4 structure. All of the XRD diffraction peaks of the MNCO can be indexed as a spinel structure phase of space group *Fd*3*m* (Figure 1). It is noted that the diffraction peaks of both the precursor and

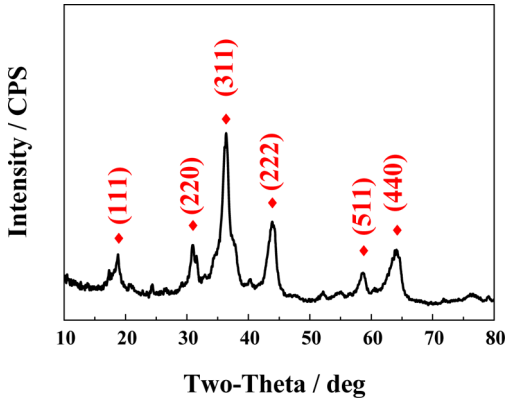

Figure 1. XRD pattern of the MNCO nanowire array.

the ternary oxide shift slightly compared to those of the $Co(OH)_2$ and spinel Co_3O_4 (PDF No. 74-1657). This is due to the differences of the metal ionic radii of Co, Mn, and Ni. However, the substitution of Mn and Ni does not affect the crystal structure of spinel Co_3O_4 significantly. Furthermore, no additional peaks for other phases are observed. The composition of MNCO nanowires is investigated through EDX (Figure S3, Supporting Information), which confirms the existence of the elements Ni, Co, Mn, O, and C (originating from the conducting resin). We operate the EDX instrument equipped with SEM, and the sample is obtained by scratching the Ni foam. Wherein the atom ratio of Ni:MnCo is 1.46:0.36:1.18, indicating that cobalt atoms are partially replaced by both nickel atoms and manganese atoms. The specific surface area of the MNCO nanowires, calculated by employing the Brunauer−Emmett−Teller (BET)

method, is found to be 84.52 m^2 g^{-1} (Figure S4, Supporting Information).

Figure 2 shows the SEM images of the MNCO nanowire array and its precursor. The morphologies of the MNCO nanowires

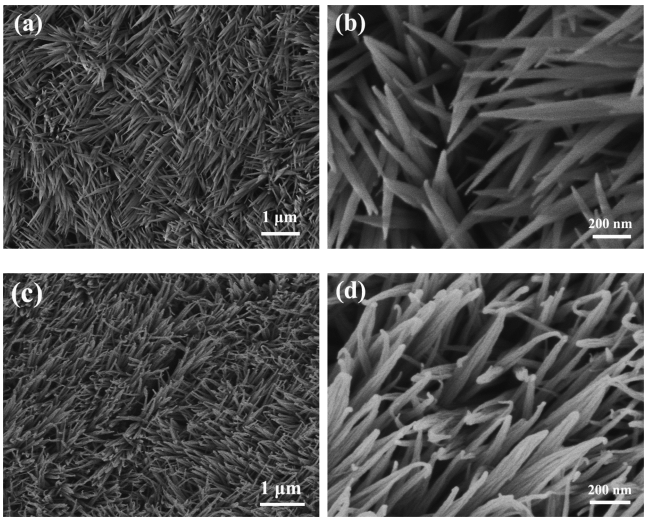

Figure 2. SEM images of (a, b) the hydroxide precursor and (c, d) the MNCO nanowire array.

and their hydroxide precursor are almost the same (Figure 2a,b), maintaining the nanowire array structure. Figure 2c,d clearly indicates that the nanowires with an average diameter of 50 nm grow directly on the nickel foam, forming a nanowire array. These nanowires dispersively distribute on the surface of Ni foam, which means the reduction of self-aggregation. From the mapping results shown in Figure 3, the three elements (Co, Mn, and Ni) distribute uniformly on each nanowire.

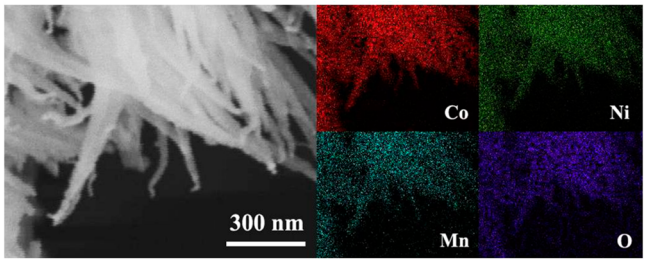

Figure 3. EDX mapping of the MNCO nanowire array.

Further insight into the detailed nanostructure is elucidated by TEM results, further confirming the nanowire architecture. The structural characterization of a single nanowire is performed in detail by HRTEM and selected-area electron diffraction (SAED). In Figure 4a, the typical TEM image confirms that the average diameter of nanowires is about 50 nm. In addition, the MNCO nanowires present a mesoporous structure, which is ascribed to the successive release and loss of CO_2 and H_2O during the thermal decomposition of the precursor. Figure 4b shows a HRTEM image of the MNCO nanowires. The lattice fringes with a lattice spacing of about 0.47 nm correspond to the (111) planes of space group *Fd*3*m*. The SAED pattern of the nanowire is also presented in Figure 4c, which confirms the polycrystalline feature of MNCO nanowires. Apparently, the SAED pattern can be well-indexed to the spinel structure. The high specific surface area and mesoporous structure of the MNCO product provide low-resistance pathways and more active sites, which can help to improve ion and electron transfer, thus leading to enhanced electrochemical performances.

3.2. Electrochemical Studies. *3.2.1. Electrode Performances.* The redox reaction mechanism for the pseudocapacitance of MNCO is described by the following equations, and the chemical transformations are highly reversible. The redox reactions in the alkaline electrolyte are based on the following equations:[37,38]

$$MNCO + H_2O + OH^- \leftrightarrow CoOOH + MnOOH + NiOOH + e^- \quad (1)$$

$$CoOOH + MnOOH + OH^- \leftrightarrow CoO_2 + MnO_2 + H_2O + e^- \quad (2)$$

CV analysis is considered to be a suitable tool for estimating the difference between the non-Faradaic and Faradaic reactions. Figure 5a shows the CV curves of the MNCO nanowire array electrode in the voltage region of 0−0.5 V (vs Ag/AgCl) at different scan rates. There is one oxidation peak, P1, observed in the anodic process and one reduction peak, P2, observed in the cathodic process, which indicates that the capacitive characteristics are mainly governed by Faradaic reaction. The observed peak potentials are centered at about 0.42 V (P1) and 0.26 V (P2) vs Ag/AgCl, respectively, at a scan rate of 50 mV s^{-1}, which may come from the reversible reactions of Mn^{2+}/Mn^{3+}, Ni^{2+}/Ni^{3+}, and Co^{2+}/Co^{3+} redox pairs in 6 M KOH aqueous solution, as the above redox reactions. With the increase of scan rate, the anodic peaks shift toward positive potential and cathodic peaks shift toward negative potential, due to the limited diffusion time,[39,40] indicating the quasireversible feature of the redox couples.

Figure 5b shows the charge−discharge curve of MNCO nanowire array within the voltage range of 0−0.5 V at a current density of 1 A g^{-1}. It can be seen that there is an obvious discharge voltage plateau in the discharge process, which indicates that the electrode exhibits pseudocapacitance behavior. According to the equation $C = I\Delta t/M\Delta V$, the specific capacitance of the MNCO nanowire array is calculated to be 638 F g^{-1} at 1 A g^{-1}. The charge−discharge curves at current densities of 1−20 A g^{-1} are shown in Figure 5c. Figure 5d shows the dependence of specific capacitance on the discharge current density. The MNCO nanowire array electrode exhibits high specific capacitance values of 609.6 F g^{-1} at 2 A g^{-1}, 566 F g^{-1} at 4 A g^{-1}, 486.4 F g^{-1} at 8 A g^{-1}, 466 F g^{-1} at 10 A g^{-1}, and 404 F g^{-1} at 20 A g^{-1}, respectively; 63.3% of the capacitance is maintained when the discharge current density increases from 1 A g^{-1} to 20 A g^{-1}. The nickel foam only exhibits small capacitance with several discharge seconds, which can be neglected.[41]

Figure 6 indicates the Ragone plot (power density vs energy density) of MNCO nanowire array electrode. The energy density can be estimated to be 79.8 Wh kg^{-1} at a power density of 250 W kg^{-1}, and its energy density is still as high as 50.5 Wh kg^{-1} at a high power density of 5 kW kg^{-1}. The cycle performance of the MNCO nanowire array is examined at a current density of 2 A g^{-1}, as presented in Figure 7. It can be observed that the specific capacitance increases gradually at the beginning of the charge−discharge cycles, which can be attributed to the complete activation process of the Faradaic pseudocapacitance of the electrode,[43] and then there is a slight decrease. The complete activation takes almost 2000 cycles; a possible explanation is that only a part of electrode material is active at first. As the electrolyte

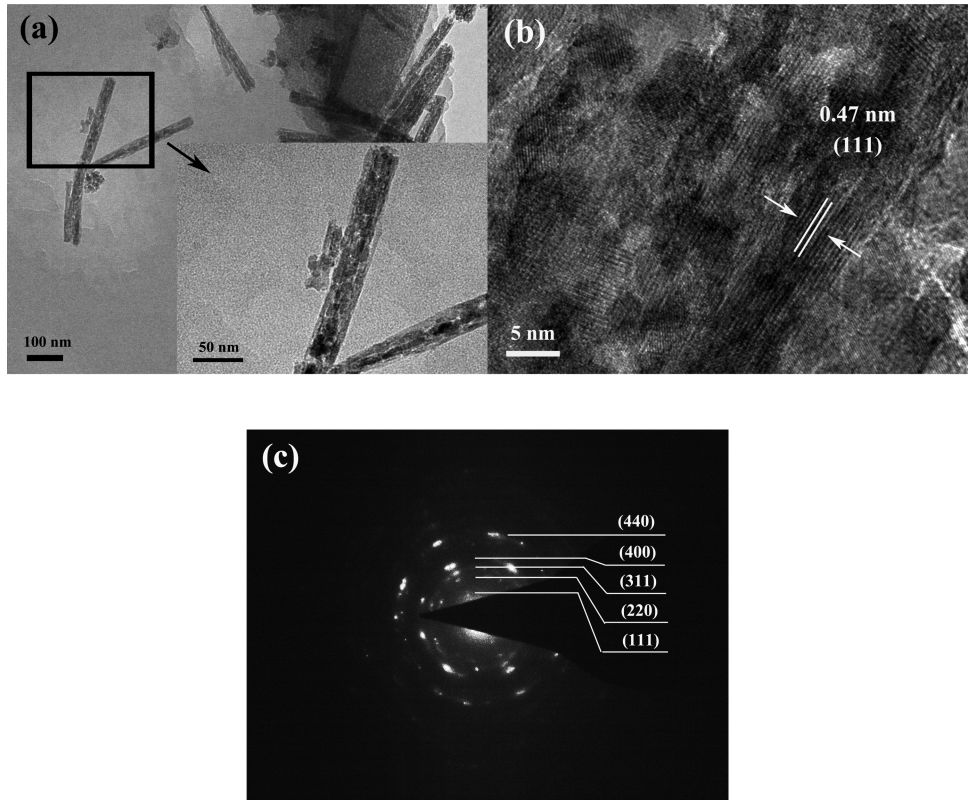

Figure 4. (a) TEM images, (b) HRTEM image, and (c) SAED pattern of the MNCO nanowire.

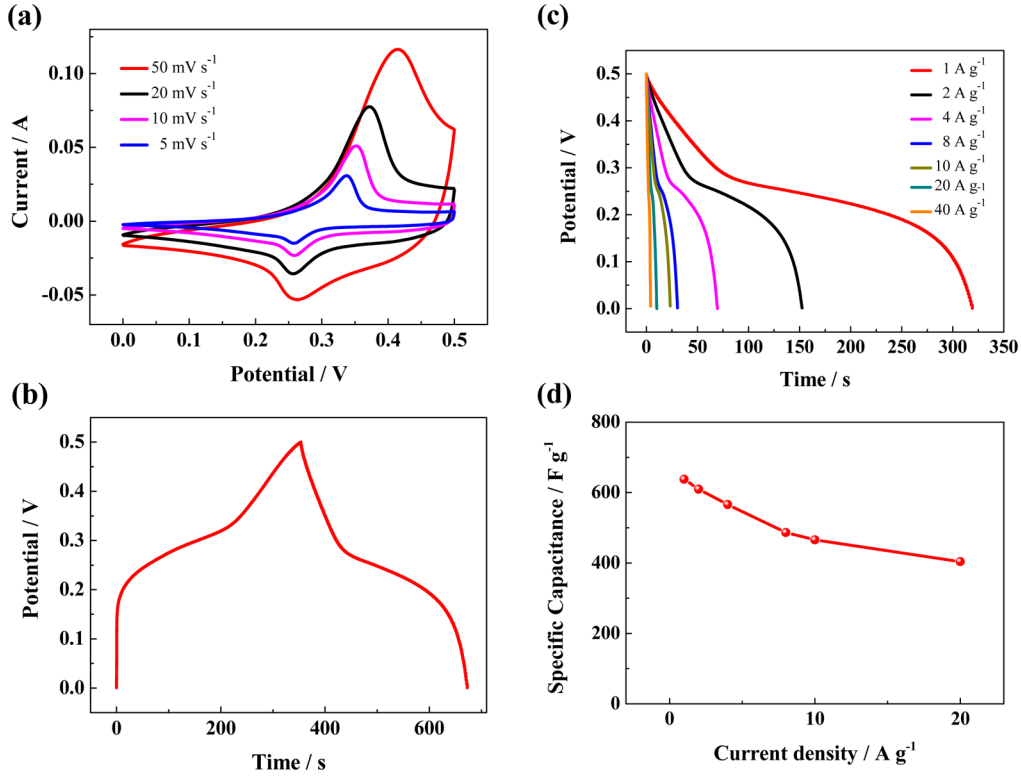

Figure 5. (a) CV curves of MNCO nanowire array electrode in the potential region of 0−0.5 V at different scan rates (vs Ag/AgCl), (b) galvanostatic charge−discharge curve of MNCO nanowire array at a current density of 1 A g^{-1}, (c) galvanostatic charge−discharge curves of MNCO nanowire array at different current densities, and (d) current density dependence of the specific capacitance.

gradually penetrates into the inner region of the electrode, more and more sites become activated and contribute to the increase of capacitance. After 6000 cycles, the electrode presents a capacitance of 703.5 F g^{-1} with 93.6% of the maximum value.

dx.doi.org/10.1021/am5048653 | ACS Appl. Mater. Interfaces 2014, 6, 18040−18047

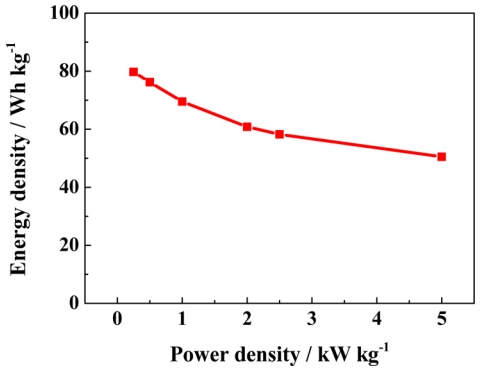

Figure 6. Ragone plot of the MNCO nanowire array electrode.

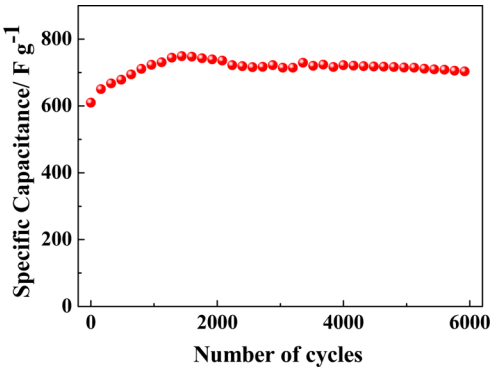

Figure 7. Cyclability of the MNCO nanowire array between 0 and 0.5 V at a current density of 2 A g^{-1} (vs Ag/AgCl).

Moreover, the nanowire array architecture is well-maintained after cycling for 4000 cycles (Figure S5, Supporting Information), which can also indicate that the nanowire array possesses good structural stability.

The excellent electrochemical performances of the MNCO array can be ascribed to its nanostructure. It is suggested that a high specific surface area and the open geometry between the nanowires allow easier electrolyte penetration and diffusion into the inner region of the electrode, resulting in high utilization of active materials and enhanced diffusion kinetics. Besides, the nanowire structure stays stable during the charge−discharge process, helping to alleviate the structural damage caused by volume expansion during cycling and maintaining the mechanical integrality of the overall electrode. All of the above lead to excellent pseudocapacitor performances.

3.2.2. Asymmetric Supercapacitor Performances. In order to explore the practice application of the MNCO electrode, the MNCO//C ASC is successfully fabricated. In the MNCO//C ASC, the weight ratio of MNCO to C is obtained from the specific capacitance of the MNCO electrode and the carbon electrode. The specific capacitance of a given electrode (MNCO or C) is determined by integrating the CV curve to obtain the voltammetric charge (Q) and subsequently dividing this charge by the mass of the electrode (m) and the width of the potential window (ΔE).[42]

$$C = Q/(\Delta E m) \tag{3}$$

Subsequently, to ensure the charge balance of the hybrid cell, the optimal weight ratio between the positive and negative electrodes is 0.89, and the active mass of the ASC includes materials of both the positive and negative electrodes.

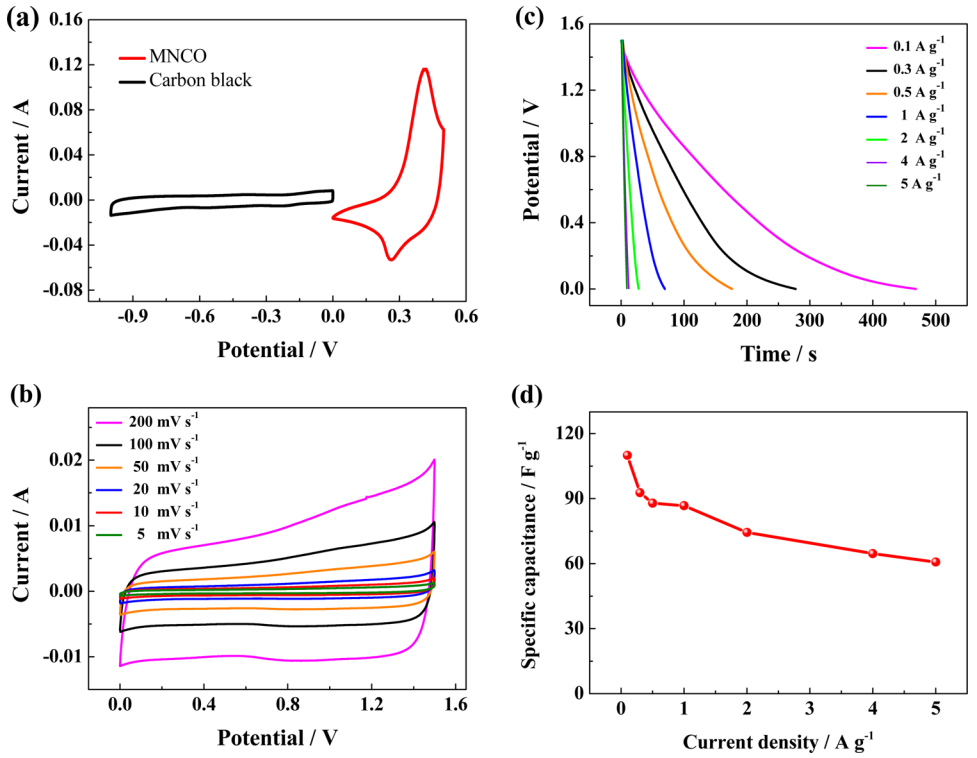

Figure 8. (a) CV curves of MNCO and carbon electrode performed in a three-electrode cell in 6 M KOH electrolyte at a scan rate of 50 mV s^{-1}, (b) CV curves of the MNCO//C ASC device measured at a potential window of 0−1.5 V at different scan rates, (c) galvanostatic discharge curves of the ASC device at different current densities, and (d) current density dependence of the specific capacitance.

dx.doi.org/10.1021/am5048653 | ACS Appl. Mater. Interfaces 2014, 6, 18040−18047

To estimate the stable potential window of MNCO//C ASC, CV measurements were performed on the two electrode materials in 6 M KOH aqueous solution before evaluating the asymmetric cell, using a three-electrode system with a platinum foil as counter electrode and Ag/AgCl electrode as reference electrode, as shown in Figure 8a. The MNCO electrode is measured within a potential window of 0−0.5 V, while the carbon electrode is measured within a potential window of −1 to 0 V at a scan rate of 50 mV s^{-1}. The CV curve of the carbon electrode exhibits a nearly rectangular shape, which is a characteristic of an electric double layer capacitor. As for the MNCO, two redox peaks are easily observed, which have already been analyzed above. On the basis of these results, it can be seen that the potential window of MNCO is from 0 to 0.5 V and the potential window of carbon is from −1 to 0 V with capacitive behavior. Furthermore, it can be observed that the two materials are stable in a different range of potentials. Therefore, the overall capacitance of the MNCO//C ASC device derives from the combined contribution of electrical double layer capacitance and redox pseudocapacitance. The total operating cell voltage can be expressed as the sum of the potential range for the two electrodes. It is possible to conclude that the cell potential can be extended up to 1.5 V in 6 M KOH aqueous solution, if the two electrodes are assembled into ASC devices. Therefore, we construct an ASC device by using MNCO as the positive electrode and carbon black as the negative electrode in a 6 M KOH electrolyte. Figure 8b shows the CV curves of our ASC device in a potential window of 0−1.5 V in 6 M KOH electrolyte at different scan rates of 200, 100, 50, 20, 10, and 5 mV s^{-1}. Compared to that of pure MNCO and carbon electrode, the ASC device shows relatively rectangular CV curves without obvious redox peaks, even at the potential up to 1.5 V, indicating the ideal capacitive behavior. In addition, CV profiles still retain a relatively rectangular shape without obvious distortion with increasing potential scan rates, indicating the desirable fast charge−discharge property for power devices. Rate capability is an important factor for the electrochemical capacitors in power applications. So we perform galvanostatic charge−discharge tests at various current densities in 6 M KOH electrolyte. A good electrochemical energy storage device is required to provide its high specific capacitance and high energy density at a high charge−discharge rate. Plots of voltage versus time for the ASC at various current densities are shown in Figure 8c. Figure 8d presents the relationship between the specific capacitance of the ASC device and current density. A linear variation of the voltage is observed, indicating that the ASC has an ideal capacitive characteristic, which is in good agreement with CV curves. On the basis of the equation $C = I\Delta t/M\Delta V$, the ASC device delivers a maximum specific capacitance of 109.9 F g^{-1} at 0.1 A g^{-1} and shows specific capacitances of 92.7 F g^{-1} (0.3 A g^{-1}), 87.9 F g^{-1} (0.5 A g^{-1}), 86.7 F g^{-1} (1 A g^{-1}), 74.4 F g^{-1} (2 A g^{-1}), 64.4 F g^{-1} (4 A g^{-1}), and 60.7 F g^{-1} (5 A g^{-1}), respectively. The specific capacitance drops 55.1% when the current density increases from 0.1 to 5 A g^{-1}. The specific capacitance gradually decreases with the increase of current density, since diffusion most likely limits the movement of ions and electrons due to the time constraint. Nevertheless, the present ASC device still retains a good rate performance.

Figure 9 shows the Ragone plot of the ASC device measured in the voltage window of 0−1.5 V. The energy and power densities are derived from the discharge curves at different current densities. For comparison, the symmetric supercapacitor devices on MNCO//MNCO and C//C are assembled and characterized

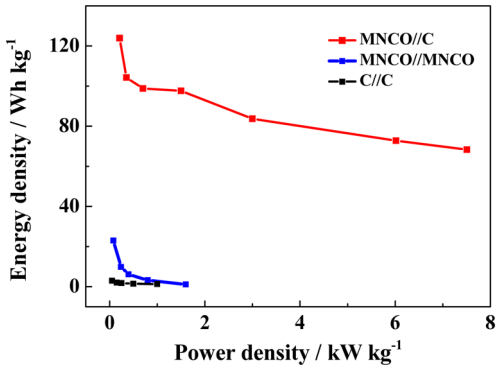

Figure 9. Ragone plots of the as-fabricated ASC device and the symmetric supercapacitors MNCO//MNCO and C//C.

in 6 M KOH electrolyte. It can be observed that the ASC device exhibits much higher energy and power densities than the symmetric supercapacitor cells. The energy density can be estimated to be 123.6 Wh kg^{-1} at a power density of 264 W kg^{-1}, and the energy density still retains 68.3 Wh kg^{-1} at a high power density of 7.5 kW kg^{-1}. The maximum energy density obtained for our ASC device with a cell voltage of 1.5 V is much higher than that of other asymmetric supercapacitors with aqueous electrolyte solutions, such as RuO_2−NPG//$Co(OH)_2$−NPG (120 Wh kg^{-1}),[43] graphene−MnO//AC (51.1 Wh kg^{-1}),[44] $Ni(OH)_2$//CNT (50.6 Wh kg^{-1}),[45] $Ni_xCo_{3-x}O_4$//AC (37.4 Wh kg^{-1}),[46] CoO@C//AC (58.9 Wh kg^{-1}),[47] PANI//MoO_3 (71.9 Wh kg^{-1}),[48] and PPy-NPG//MnO_2−NPG (86 Wh kg^{-1}).[49] Although the energy densities reduce with the increasing power densities, the energy density of the MNCO//C ASC device at the same power density is higher than most of the other ASCs reported, which means that the ASC device can exhibit both high energy and high power density.

A long cycling test was carried out between 0 and 1.5 V over 6000 cycles at a current density of 2 A g^{-1}. Figure 10 presents the

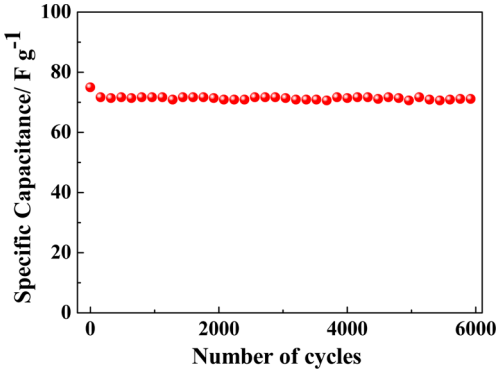

Figure 10. Cycling performance of the MNCO//C ASC device.

specific capacitance of the ASC device as a function of cycle number. The specific capacitance remains almost constant. After galvanostatic charge−discharge for 6000 cycles, the ASC device presents a capacitance of 71.4 F g^{-1} with 95.2% of the maximum value, indicating that the high stability of our ASC device is suitable for high-performance supercapacitor applications. EIS measurements were used to investigate the resistance change of the asymmetric supercapacitor before and after cycling. The Nyquist plots measured before and after 4000 cycles are displayed in Figure S6 (Supporting Information). The Nyquist plots consist of a depressed semicircle and a long low-frequency

line, and the intercept on the Z real axis in the high-frequency region corresponds to the resistance of electrolyte (R_s). The semicircle in the middle frequency range indicates the charge-transfer resistance (R_{ct}), relating to charge transfer through the electrode−electrolyte interface.[50] After 4000 cycles, only a slight increase of R_{ct} is observed.

Several contributing factors are considered for the high specific capacitance and high energy density of the ASC device: First, the energy density of electrochemical capacitors is proportional to the square of operating voltage. The voltage range of our ASC devise is extended to 1.5 V, consequently resulting in a significantly increase in energy density.[51,52] Second, the nanowire structure with large specific area ensures the high utilization of active materials, fast ion and electron transfer, and good structural stability, further decreasing the kinetic limitations of the pseudocapacitive electrode and hence resulting in the high specific capacitance and energy density of our ASC device. Third, the carbon material in the negative electrode, which is widely used as a conductive additive in electrochemical systems, possesses excellent electric conductivity as an electric double layer capacitor electrode. Apart from, the synergistic effect of the two electrodes is also an important contributing factor of the excellent electrochemical performances of the ASC device.

4. CONCLUSIONS

A highly crystalline Mn−Ni−Co ternary oxide nanowire array was synthesized by a facile hydrothermal method. The MNCO nanowire array electrode delivers noticeable pseudocapacitive performance with a high capacitance of 638 F g^{-1} at 1 A g^{-1} and an capacitance retention of 93.6% after 6000 cycles. For more practical application, a novel and durable ASC on MNCO//C is fabricated, and the device shows electrochemical capacitance performance within a voltage range of 0−1.5 V and exhibits high specific capacitance from 109.9 to 60.7 F g^{-1} as the current density increases from 0.1 to 5 A g^{-1}, as well as high energy density and good electrochemical stability. The MNCO nanowire array is expected to be a promising candidate for application in high-performance electrochemical capacitors, and the as-fabricated ASC also shows great potential in the development of energy storage devices with high energy and power densities.

■ ASSOCIATED CONTENT

Supporting Information

Illustration of the scheme of the MNCO//C asymmetric supercapacitor, XRD pattern of MNCO precursor, EDX spectrum of MNCO nanowire array, nitrogen adsorption and desorption isotherms of MNCO nanowire array, SEM image of MNCO nanowire array for supercapacitor after 4000 cycles, and Nyquist plots of MNCO//C ASC device before and after 4000 cycles. This material is available free of charge via the Internet at http://pubs.acs.org.

■ AUTHOR INFORMATION

Corresponding Author

*Tel: +86 571 87952856. Fax: +86 571 87952573. E-mail: tujp@zju.edu.cn; tujplab@zju.edu.cn.

Notes

The authors declare no competing financial interest.

■ ACKNOWLEDGMENTS

This work was supported by the Program for Innovative Research Team in University of Ministry of Education of China (IRT13037) and Key Science and Technology Innovation Team of Zhejiang Province (2010R50013).

■ REFERENCES

(1) Miller, J. R.; Simon, P. Materials Science—Electrochemical Capacitors for Energy Management. *Science* **2008**, *321*, 651−652.
(2) Yang, S. N.; Cheng, K.; Huang, J. C.; Ye, K.; Xu, Y.; Cao, D. X.; Zhang, X. M.; Wang, G. L. High-Capacitance MnO_2 Nanoflakes on Preformed C/TiO_2 Shell/Core Nanowire Arrays for Electrochemical Energy Storage. *Electrochim. Acta* **2014**, *120*, 416−422.
(3) Liu, J. P.; Jiang, J.; Bosman, M.; Fan, H. J. Three-Dimensional Tubular Arrays of MnO_2−NiO Nanoflakes with High Areal Pseudocapacitance. *J. Mater. Chem.* **2012**, *22*, 2419−2426.
(4) Xia, X. H.; Tu, J. P.; Zhang, Y. Q.; Wang, X. L.; Gu, C. D.; Zhao, X. B.; Fan, H. J. High-Quality Metal Oxide Core/Shell Nanowire Arrays on Conductive Substrates for Electrochemical Energy Storage. *ACS Nano* **2012**, *6*, 5531−5538.
(5) Dong, X. C.; Xu, H.; Wang, X. W.; Huang, Y. X.; Chan-Park, M. B.; Zhang, H.; Wang, L. H.; Huang, W.; Chen, P. 3D Graphene−Cobalt Oxide Electrode for High-Performance Supercapacitor and Enzymeless Glucose Detection. *ACS Nano* **2012**, *6*, 3206−3213.
(6) Xia, X. H.; Zhang, Y. Q.; Chao, D. L.; Cao, G.; Zhang, Y. J.; Li, L.; Ge, X.; Mínguez Bacho, I.; Tu, J. P.; Fan, H. J. Solution Synthesis of Metal Oxides for Electrochemical Energy Storage Applications. *Nanoscale* **2014**, *6*, 5008−5048.
(7) Vialat, P.; Mousty, C.; Taviot-Gueho, C.; Renaudin, G.; Martinez, H.; Dupin, J. C.; Elkaim, E.; Leroux, F. High-Performing Monometallic Cobalt Layered Double Hydroxide Supercapacitor with Defined Local Structure. *Adv. Funct. Mater.* **2014**, *24*, 4831−4842.
(8) Xia, X. H.; Tu, J. P.; Zhang, Y. Q.; Chen, J.; Wang, X. L.; Gu, C. D.; Guan, C.; Luo, J. S.; Fan, H. J. Porous Hydroxide Nanosheets on Preformed Nanowires by Electrodeposition: Branched Nanoarrays for Electrochemical Energy Storage. *Chem. Mater.* **2012**, *24*, 3793−3799.
(9) Tang, P. Y.; Han, L. J.; Zhang, L. Facile Synthesis of Graphite/PEDOT/ MnO_2 Composites on Commercial Supercapacitor Separator Membranes as Flexible and High-Performance Supercapacitor Electrodes. *ACS Appl. Mater. Interfaces* **2014**, *6*, 10506−10515.
(10) Shi, Y.; Pan, L. J.; Liu, B. R.; Wang, Y. Q.; Cui, Y.; Bao, Z. N.; Yu, G. H. Nanostructured Conductive Polypyrrole Hydrogels as High-Performance, Flexible Supercapacitor Electrodes. *J. Mater. Chem. A* **2014**, *2*, 6086−6091.
(11) Fang, X. L.; Zang, J.; Wang, X. L.; Zheng, M. S.; Zheng, N. F. A Multiple Coating Route to Hollow Carbon Spheres with Foam-Like Shells and Their Applications in Supercapacitor and Confined Catalysis. *J. Mater. Chem. A* **2014**, *2*, 6191−6197.
(12) Lu, Y.; Liu, J. K.; Liu, X. Y.; Huang, S.; Wang, T. Q.; Wang, X. L.; Gu, C. D.; Tu, J. P.; Mao, S. X. Facile Synthesis of Ni-Coated Ni_2P for Supercapacitor Applications. *CrystEngComm* **2013**, *15*, 7071−7079.
(13) Dam, D. T.; Wang, X.; Lee, J. M. Graphene/NiO Nanowires: Controllable One-Pot Synthesis and Enhanced Pseudocapacitive Behavior. *ACS Appl. Mater. Interfaces* **2014**, *6*, 8246−8256.
(14) Liu, X. M.; Long, Q.; Jiang, C. H.; Zhan, B. B.; Li, C.; Liu, S. J.; Zhao, Q.; Huang, W.; Dong, X. C. Facile and Green Synthesis of Mesoporous Co_3O_4 Nanocubes and Their Applications for Supercapacitors. *Nanoscale* **2013**, *5*, 6525−6529.
(15) Izadi-Najafabadi, A.; Yasuda, S.; Kobashi, K.; Yamada, T.; Futaba, D. N.; Hatori, H.; Yumura, M.; Iijima, S.; Hata, K. Extracting the Full Potential of Single-Walled Carbon Nanotubes as Durable Supercapacitor Electrodes Operable at 4 V with High Power and Energy Density. *Adv. Mater.* **2010**, *22*, E235−241.
(16) Yang, P. H.; Ding, Y.; Lin, Z. Y.; Chen, Z. W.; Li, Y. Z.; Qiang, P. F.; Ebrahimi, M.; Mai, W.; Wong, C. P.; Wang, Z. L. Low-Cost High-Performance Solid-State Asymmetric Supercapacitors Based on MnO_2 Nanowires and Fe_2O_3 Nanotubes. *Nano Lett.* **2014**, *14*, 731−736.

(17) Dubal, D. P.; Gund, G. S.; Holze, R.; Lokhande, C. D.; Park, C. J. Surfactant-Assisted Morphological Tuning of Hierarchical CuO Thin Films for Electrochemical Supercapacitors. *Dalton Trans.* **2013**, *42*, 6459−6467.
(18) Zhang, Y. X.; Huang, M.; Li, F.; Wang, X. L.; Wen, Z. Y. One-Pot Synthesis of Hierarchical MnO_2-Modified Diatomites for Electrochemical Capacitor Electrodes. *J. Power Sources* **2014**, *246*, 449−456.
(19) Zhou, Y.; Lachman, N.; Ghaffari, M.; Xu, H. P.; Bhattacharyya, D.; Fattahi, P.; Abidian, M. R.; Wu, S.; Gleason, K.; Wardle, B.; Zhang, Q. M. A High Performance Hybrid Asymmetric Supercapacitor via Nano-Scale Morphology Control of Graphene, Conducting Polymer, and Carbon Nanotube Electrodes. *J. Mater. Chem. A* **2014**, *2*, 9964−9969.
(20) Jiang, H.; Ma, J.; Li, C. Z. Mesoporous Carbon Incorporated Metal Oxide Nanomaterials as Supercapacitor Electrodes. *Adv. Mater.* **2012**, *24*, 4197−4202.
(21) Westover, A. S.; Tian, J. W.; Bernath, S.; Oakes, L.; Edwards, R.; Shabab, F. N.; Chatterjee, S.; Anilkumar, A. V.; Pint, C. L. A Multifunctional Load-Bearing Solid-State Supercapacitor. *Nano Lett.* **2014**, *14*, 3197−3202.
(22) Chen, P. C.; Shen, G. Z.; Shi, Y.; Chen, H. T.; Zhou, C. W. Preparation and Characterization of Flexible Asymmetric Supercapacitors Based on Transition-Metal-Oxide Nanowire/Single-Walled Carbon Nanotube Hybrid Thin-Film Electrodes. *ACS Nano* **2010**, *4*, 4403−4411.
(23) Wang, Y. Y.; Lei, Y.; Li, J.; Gu, L.; Yuan, H. Y.; Xiao, D. Synthesis of 3D-Nanonet Hollow Structured Co_3O_4 for High Capacity Supercapacitor. *ACS Appl. Mater. Interfaces* **2014**, *6*, 6739−6747.
(24) Zhang, Y. Q.; Li, L.; Shi, S. J.; Xiong, Q. Q.; Zhao, X. Y.; Wang, X. L.; Gu, C. D.; Tu, J. P. Synthesis of Porous Co_3O_4 Nanoflake Array and Its Temperature Behavior as Pseudo-Capacitor Electrode. *J. Power Sources* **2014**, *256*, 200−205.
(25) Guan, Q.; Cheng, J. L.; Wang, B.; Ni, W.; Gu, G. F.; Li, X. D.; Huang, L.; Yang, G. C.; Nie, F. D. Needle-like Co_3O_4 Anchored on the Graphene with Enhanced Electrochemical Performance for Aqueous Supercapacitors. *ACS Appl. Mater. Interfaces* **2014**, *6*, 7626−7632.
(26) Vijayakumar, S.; Nagamuthu, S.; Muralidharan, G. Porous NiO/C Nanoconnposites as Electrode Material for Electrochemical Supercapacitors. *ACS Sustainable Chem. Eng.* **2013**, *1*, 1110−1118.
(27) Yang, Z. H.; Xu, F. F.; Zhang, W. X.; Mei, Z. S.; Pei, B.; Zhu, X. Controllable Preparation of Multishelled NiO Hollow Nanospheres via Layer-by-Layer Self-Assembly for Supercapacitor Application. *J. Power Sources* **2014**, *246*, 24−31.
(28) Xia, X. H.; Tu, J. P.; Wang, X. L.; Gu, C. D.; Zhao, X. B. Hierarchically Porous NiO Film Grown by Chemical Bath Deposition via Colloidal Crystal Template as Electrochemical Pseudocapacitor Material. *J. Mater. Chem.* **2011**, *21*, 671−679.
(29) Meher, S. K.; Justin, P.; Rao, G. R. Nanoscale Morphology Dependent Pseudocapacitance of NiO: Influence of Intercalating Anions during Synthesis. *Nanoscale* **2011**, *3*, 683−692.
(30) Qu, Q. T.; Zhang, P.; Wang, B.; Chen, Y. H.; Tian, S.; Wu, Y. P.; Holze, R. Electrochemical Performance of MnO_2 Nanorods in Neutral Aqueous Electrolytes as a Cathode for Asymmetric Supercapacitors. *J. Phys. Chem. C* **2009**, *113*, 14020−14027.
(31) Ghimbeu, C. M.; Malak-Polaczyk, A.; Frackowiak, E.; Vix-Guterl, C. Template-Derived High Surface Area λ-MnO_2 for Supercapacitor Applications. *J. Appl. Electrochem.* **2014**, *44*, 123−132.
(32) Grote, F.; Kuhnel, R. S.; Balducci, A.; Lei, Y. Template Assisted Fabrication of Free-Standing MnO_2 Nanotube and Nanowire Arrays and Their Application in Supercapacitors. *Appl. Phys. Lett.* **2014**, *104*, 053904.
(33) Tadjer, M. J.; Mastro, M. A.; Rojo, J. M.; Mojena, A. B.; Calle, F.; Kub, F. J.; Eddy, C. R. MnO_2-Based Electrochemical Supercapacitors on Flexible Carbon Substrates. *J. Electron. Mater.* **2014**, *43*, 1188−1193.
(34) Ren, Y. M.; Xu, Q.; Zhang, J. M.; Yang, H. X.; Wang, B.; Yang, D. Y.; Hu, J. H.; Liu, Z. M. Functionalization of Biomass Carbonaceous Aerogels: Selective Preparation of MnO_2@CA Composites for Supercapacitors. *ACS Appl. Mater. Interfaces* **2014**, *6*, 9689−9697.
(35) Zhang, Y. F.; Ma, M. Z.; Yang, J.; Su, H. Q.; Huang, W.; Dong, X. C. Selective Synthesis of Hierarchical Mesoporous Spinel $NiCo_2O_4$ for High-Performance Supercapacitors. *Nanoscale* **2014**, *6*, 4303−4308.
(36) Gomez, J.; Kalu, E. E. High-Performance Binder-Free Co−Mn Composite Oxide Supercapacitor Electrode. *J. Power Sources* **2013**, *230*, 218−224.
(37) Li, L.; Zhang, Y. Q.; Liu, X. Y.; Shi, S. J.; Zhao, X. Y.; Zhang, H.; Ge, X.; Cai, G. F.; Gu, C. D.; Wang, X. L.; Tu, J. P. One-Dimension $MnCo_2O_4$ Nanowire Arrays for Electrochemical Energy Storage. *Electrochim. Acta* **2014**, *116*, 467−474.
(38) Liu, X. Y.; Shi, S. J.; Xiong, Q. Q.; Li, L.; Zhang, Y. J.; Tang, H.; Gu, C. D.; Wang, X. L.; Tu, J. P. Hierarchical $NiCo_2O_4$@$NiCo_2O_4$ Core/Shell Nanoflake Arrays as High-Performance Supercapacitor Materials. *ACS Appl. Mater. Interfaces* **2013**, *5*, 8790−8795.
(39) Duan, B. R.; Cao, Q. Hierarchically Porous Co_3O_4 Film Prepared by Hydrothermal Synthesis Method Based on Colloidal Crystal Template for Supercapacitor Application. *Electrochim. Acta* **2012**, *64*, 154−161.
(40) Toupin, M.; Brousse, T.; Bélanger, D. Influence of Microstucture on the Charge Storage Properties of Chemically Synthesized Manganese Dioxide. *Chem. Mater.* **2002**, *14*, 3946−3952.
(41) Kim, S. H.; Kim, Y. I.; Park, J. H.; Ko, J. M. Cobalt−Manganese Oxide/Carbon-Nanofiber Composite Electrodes for Supercapacitors. *Int. J. Electrochem. Sci.* **2009**, *4*, 1489−1496.
(42) Du, X.; Wang, C. Y.; Chen, M. M.; Jiao, Y.; Wang, J. Electrochemical Performances of Nanoparticle Fe_3O_4/Activated Carbon Supercapacitor Using KOH Electrolyte Solution. *J. Phys. Chem. C* **2009**, *113*, 2643−2646.
(43) Chen, L. Y.; Hou, Y.; Kang, J. L.; Hirata, A.; Chen, M. W. Asymmetric Metal Oxide Pseudocapacitors Advanced by Three-Dimensional Nanoporous Metal Electrodes. *J. Mater. Chem. A* **2014**, *2*, 8448−8455.
(44) Fan, Z. J.; Yan, J.; Wei, T.; Zhi, L. J.; Ning, G. Q.; Li, T. Y.; Wei, F. Asymmetric Supercapacitors Based on Graphene/MnO_2 and Activated Carbon Nanofiber Electrodes with High Power and Energy Density. *Adv. Funct. Mater.* **2011**, *21*, 2366−2375.
(45) Tang, Z.; Tang, C. H.; Gong, H. A High Energy Density Asymmetric Supercapacitor from Nano-Architectured $Ni(OH)_2$/Carbon Nanotube Electrodes. *Adv. Funct. Mater.* **2012**, *22*, 1272−1278.
(46) Wang, X.; Yan, C. Y.; Sumboja, A.; Lee, P. S. High Performance Porous Nickel Cobalt Oxide Nanowires for Asymmetric Supercapacitor. *Nano Energy* **2014**, *3*, 119−126.
(47) Wang, H.; Qing, C.; Guo, J. L.; Aref, A. A.; Sun, D. M.; Wang, B. X.; Tang, Y. W. Highly Conductive Carbon−CoO Hybrid Nanostructure Arrays with Enhanced Electrochemical Performance for Asymmetric Supercapacitors. *J. Mater. Chem. A* **2014**, *2*, 11776−11783.
(48) Peng, H.; Ma, G. F.; Mu, J. J.; Sun, K. J.; Lei, Z. Q. Low-Cost and High Energy Density Asymmetric Supercapacitors Based on Polyaniline Nanotubes and MoO_3 Nanobelts. *J. Mater. Chem. A* **2014**, *2*, 10384−10388.
(49) Hou, Y.; Chen, L. Y.; Liu, P.; Kang, J. L.; Fujita, T.; Chen, M. W. Nanoporous Metal Based Flexible Asymmetric Pseudocapacitors. *J. Mater. Chem. A* **2014**, *2*, 10910−10916.
(50) Gao, H. C.; Xiao, F.; Ching, C. B.; Duan, H. W. High-Performance Asymmetric Supercapacitor Based on Graphene Hydrogel and Nanostructured MnO_2. *ACS Appl. Mater. Interfaces* **2012**, *4*, 2801−2810.
(51) Frackowiak, E.; Béguin, F. Carbon Materials for the Electrochemical Storage of Energy in Capacitors. *Carbon* **2001**, *39*, 937−950.
(52) Kötz, R.; Carlen, M. Principles and Applications of Electrochemical Capacitors. *Electrochim. Acta* **2000**, *45*, 2483−2498.